Microstructural Investigations of the White and Deformed Layers Close to the Turned Surface of Ti-6Al-4V

MICKAEL RANCIC, CHRISTOPHE COLIN, MOHAMED SENNOUR, JEAN-PHILLIPE COSTES, and GÉRARD POULACHON

In the aircraft industry, along with geometrical and dimensional integrity, the surface integrity of manufactured parts is a necessity. In fact, severe anomalies generated during machining may have a substantial impact on the lifetime of the parts. Nevertheless, these anomalies are not well known in terms of microstructures such as the white layer in titanium alloys. Based on this observation, the present paper deals with microstructural investigations performed on Ti-6Al-4V white and deformed layers generated during turning with a round uncoated carbide insert. The aim of this study is to characterize these anomalies in terms of microstructure and phases. In particular, this study provides a better understanding of metallurgical transformations in the sublayer of machined surfaces through qualitative models.

I. INTRODUCTION

TITANIUM and its alloys are largely used in many industrial domains, such as aerospace or surgical implants, due to their thermomechanical characteristics and their resistance.[1] Nevertheless, it is known as a material which is difficult to cut.[2] The poor machinability of titanium alloys is mainly due to their thermomechanical properties. In particular, their low Young modulus induces a significant elastic recovery after machining, leading to significant rubbing of the tool flank face on the freshly machined surface. The combination of this high mechanical loading and the high temperature reached during machining due to low thermal conductivity[3] can generate severe anomalies on the part.

Generally, two types of anomaly are observed in the sublayer of a Ti-6Al-4V machined surface. The first is a deformed layer. This damage consists of the plastic deformation of the material grains. The depth of the deformed layer can reach almost ten micrometers on a Ti-6Al-4V part turned with uncoated carbide tools.[4] The second kind of anomaly generated on Ti-6Al-4V is called the ''white layer'' or transformed layer. This damage is unacceptable because it leads to a large decrease in part lifetime. The white layer is always combined with a deformed layer, as observed on a Ti-6Al-4V sample drilled with coated carbide tool[5] or on Ti-6Al-4V turned with a PolyCrystalline Diamond (PCD) tool.[6] In both studies,[5,6] this white layer is located on the top layer (the nearest sublayer to the machined surface), and the deformed layer is located below. Cantero *et al.*[5] supposed the white layer to be rich in oxygen, which implies the generation of alpha case close to drilled surface. The presence of oxygen contamination was attributed to the high temperature reached during machining. However, no chemical analysis has confirmed this assumption.

Few metallurgical studies have investigated that this white layer generated in freshly machined Ti-6Al-4V parts. The microstructure of this anomaly is only observed in chips: the adiabatic shear band (similar to that observed within the chip) evolves from a deformed layer to a transformed layer, composed of martensitic α'' as the cutting speed increases.[7] These transformed and deformed layers are studied in different domains, such as ballistics[8–12] or high strain rate deformation tests,[13–15] where the strain and the strain rate are close to those obtained during machining. According to these studies, microstructural evolution and phase transformation are observed on deformed and transformed layers. All of the authors confirm that the adiabatic shear band is composed of recrystallized grains.

In the literature, no study deals with the chemical composition and the microstructural characteristics of the white and deformed layers generated in the top layer of a Ti-6Al4V turned surface. For this reason, in this article, the deformed and the white layers generated during Ti-6Al-4V turning are investigated. Scanning electron microscopy (SEM), transmission electron microscopy (TEM), and wave dispersion spectroscopy were performed in order to identify the microstructural

MICKAEL RANCIC, Machining Process Engineer, is with the Department of Machining, SNECMA, Route Henri Auguste Desbruères BP 81, 91003 Evry Cedex, France, and also with MINES ParisTech, PSL Research University, MAT- Centre des matériaux, CNRS UMR 7633, BP 87, 91003 Evry, France, and also with LaBoMaP, Arts et Metiers ParisTech, Rue porte de Paris, Cluny 71250, France. Contact e-mail: mickael.rancic@safrangroup.com CHRISTOPHE COLIN and MOHAMED SENNOUR, Associate Professors, are with MINES ParisTech, PSL Research University. JEAN-PHILLIPE COSTES, Associate Professor, and GÉRARD POULACHON, Full Professor, are with LaBoMaP, Arts et Metiers ParisTech.

variation, and the phase transformation of the thermo-mechanically affected material. The results of these investigations are compared to those obtained during ballistic and high strain rate deformation tests. Prior to these metallurgical investigations, turning tests were performed to define the severe cutting conditions enabling the generation of substantial deformed and white layers.

II. EXPERIMENTAL SET-UP

A. *Material*

The material used during the tests was a wrought and annealed Ti-6Al-4V alloy bar. Its main mechanical properties and chemical composition are summarized in Tables I and II, respectively. The microstructure of this alloy, revealed with Kroll chemical etching, is bimodal. It presents 20 μm α and $\alpha + \beta$ equiaxial grains. The α grains are composed of globular primary α and the remainder of lamellar secondary α and lamellar β phases. At room temperature, the volume fractions of the α and β phases are 96 and 4 pct, respectively. The average hardness value of this alloy is 315.5 HV_{20}. The β-transus is in a range between 1253 K and 1283 K (980 °C and 1010 °C).

B. *Insert and Facilities*

A 5-mm round uncoated carbide insert without a chip breaker was used for the machining tests. The ISO designation of this insert is LCGR1705M0-0500-RP, 883. Both clearance and rake angles were 6 deg. The tool edge radius was between 20 and 25 μm. The grade of this carbide tool was K20, which corresponds to a 6 wt pct cobalt binder, with a hardness value close to 1630 ± 20 HV_1. This insert was composed of a large distribution of WC carbide sizes. Most WC carbides are of submicrometric sizes (0.5 to 0.8 μm), and the remainders are medium (1.3 to 2.5 μm) or coarse (2.5 to 6 μm). Table III summarizes the main metallurgical and geometrical characteristics of the round insert used during testing. The diameter of the machined sample was 205 mm. The lubricant used was a 10 pct water soluble Blasocut 2000 CF oil, and the lathe was a 24 kW power spindle.

C. *Experimental Approach*

Cutting conditions which generate severe anomalies on the top layer of the machined surface are difficult to determine. Moreover, the thickness of these anomalies has to be sufficient to be investigated. In order to define these cutting conditions, it is assumed that the domain named Tool Material Pair (TMP) is equivalent to the domain without anomalies. In addition, machining performed using cutting conditions within this domain does not induce anomalies in the material.

The tool material pair method is based on the minimization of cutting energy with respect to the cutting conditions. This method is described in the AFNOR NF E 66-520-8 standard. For turning operations, it consists of determining a range of cutting conditions within which the specific cutting pressure (Kc) has the lowest values. This parameter represents the value of the average macroscopic pressure experienced by the rake in the tangential direction. This value is calculated from the tangential force (Ft), measured with a piezoelectric dynamometer, and derived from the following equation (Eq. [1]):

$$Kc = \frac{Ft}{(d.o.c) \times f} \qquad [1]$$

with $d.o.c.$ depth of cut (mm), f feed (mm/rev), Ft (N), and Kc (MPa).

Three series of tests were performed. For each series, only one cutting parameter was varied while the others were fixed. In the case of turning, the cutting speed (Vc), the feed, and the depth of cut were studied. The low threshold of the TMP domain regarding feed and depth of cut was 0.18 mm/rev and 0.11 mm, respectively. The two other thresholds, regarding cutting speed, were 105 and 285 m/min. According to Chou,[17] the cutting parameters having the most impact for steel are the feed and, above all, the cutting speed. Thus, in order to be certain to generate severe and large anomalies (especially the white layer), it was decided to use the following cutting parameters outside the TMP domain taking into account the cutting speed: $Vc = 450$ m/minutes, $f = 0.375$ mm/rev and $d.o.c = 0.5$ mm. The machining length was 10 mm (in the cutting direction).

D. *Microstructural Investigations*

SEM and electron probe micro-analysis (EPMA) investigations were carried out, respectively, using a Zeiss DSM 982 microscope equipped with a field-emission gun and a CAMECA SX100 micro-analyzer.

TEM observations were carried out using a FEI TECNAI F20-ST field-emission gun microscope equipped with an energy dispersive X-ray (EDX) device, a scanning TEM (STEM) system, and high-angle annular dark field (HAADF) detector. The STEM-HAADF combination enabled us to obtain chemical contrast (Z-contrast) images with a high spatial

Table I. Mechanical Properties of Wrought Ti-6Al-4V Material[16]

E	Young Modulus	110 (GPa)
$\sigma y_{0,2}$ pct	0.2 pct yield strength	920 MPa
σu	ultimate tensile strength	990 MPa
A pct	elongation	14 pct

Table II. Chemical Composition of the Studied Ti-6Al-4V Alloy

Elements	Ti	Al	V	Fe Max.	O Max.
Composition (wt pct)	—	5.5 6.75	3.5–4.5	0.3	0.13

Table III. Main Metallurgical and Geometrical Characteristics of the Round Insert

γ_0	α_0	D_{out}	Coating	Grade	Co (pct)	Hardness	Average WC Carbide Size	Cutting Edge Radius
6 deg	6 deg	5 mm	None	ISO K20	6 wt pct	1630 ± 21 HV_1	1,5 μm	20 to 25 μm

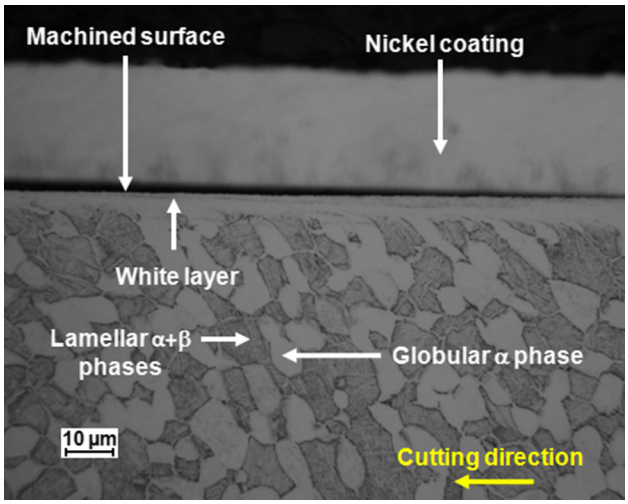

Fig. 1—Optical image showing a cross-section view of the top layer below the machined surface.

resolution. EDX analyses were performed in both positional and line-scan modes using a nanometric probe size (1 to 2 nm). The crystallographic structure of different phases was investigated using electron diffraction.

Two TEM samples were observed. The first was extracted from bulk material (undamaged zone) and prepared by ion milling on a Gatan® PIPS device. The second sample was extracted directly from the machined surface using the focused ion beam (FIB) technique on a dual beam FEI Strata DB400 apparatus. FIB preparation was chosen to protect the white and deformed layers from being abraded during mechanical polishing.

III. RESULTS

A. *Optical and Scanning Electron Microscopy (SEM) Investigations*

Figure 1 shows a cross-section of the machined surface top layer in the cutting direction after Kroll chemical etching. The white layer is clearly visible just below the machined surface. However, at this scale, the detailed microstructure of this damage cannot be defined. Below the white layer, a deformed layer composed of elongated α globular and $\alpha + \beta$ lamellar grains is observed.

Observation using a scanning electron microscope shows that the white layer seems to be composed of randomly oriented needles (Figures 2(a) and (b)). The old grain boundaries are no longer visible. This acicular microstructure could be that of the martensitic phase. The generation of this phase in Ti-6Al-4V is due to rapid quenching from the β domain above the β-transus. According to Ahmed and Rack,[18] the α' needles formed during this rapid quenching [$V_{Quenching} > 673$ K/s (400 °C/s)] are orthogonal to each other inside the same grain. Since the grains within the white layer are not defined, SEM investigations do not allow any conclusions to be made about the nature of these generated phases.

Within the undamaged zone (Figure 2(c)), globular α and lamellar $\alpha + \beta$ phases are clearly identified, with the α phase exhibiting a darker contrast compared to the β phase, conversely to what is observed in the optical micrograph.

B. *Electron Microprobe Analysis (EPMA) Investigations*

Figure 3(a) presents a SEM micrograph of the sublayer of the machined surface. A lap composed of the white layer is observed on the surface. Figures 3(b) through (d) shows the corresponding electron microprobe cartographies of titanium, aluminum, and vanadium, respectively. Elemental maps reveal that titanium is almost homogeneous on the white layer and within the underlying sublayer. In the bulk material and within the deformed layer, the different phases can be distinguished due to their different chemical compositions: the α globular and lamellar phases have greater aluminum content, whereas vanadium is predominant in the β lamellar phases. As the chemical composition of the white layer is almost homogeneous, it could be considered as a single-phase layer. The amount of aluminum and vanadium in this single-phase layer is smaller than in the bulk material and in the deformed layer. This is due to the formation of a new phase, as described in the following section. Contrary to Cantero *et al.*[5] study, EPMA investigations have not revealed any evidence of oxygen diffusion within the single-phase layer.

The chemical compositions of the α, β phases and the single-phase layer are summarized in Table IV. As the beam diameter is larger than the lamellar phase width, their chemical composition is approximate. These results confirm that the chemical composition of the

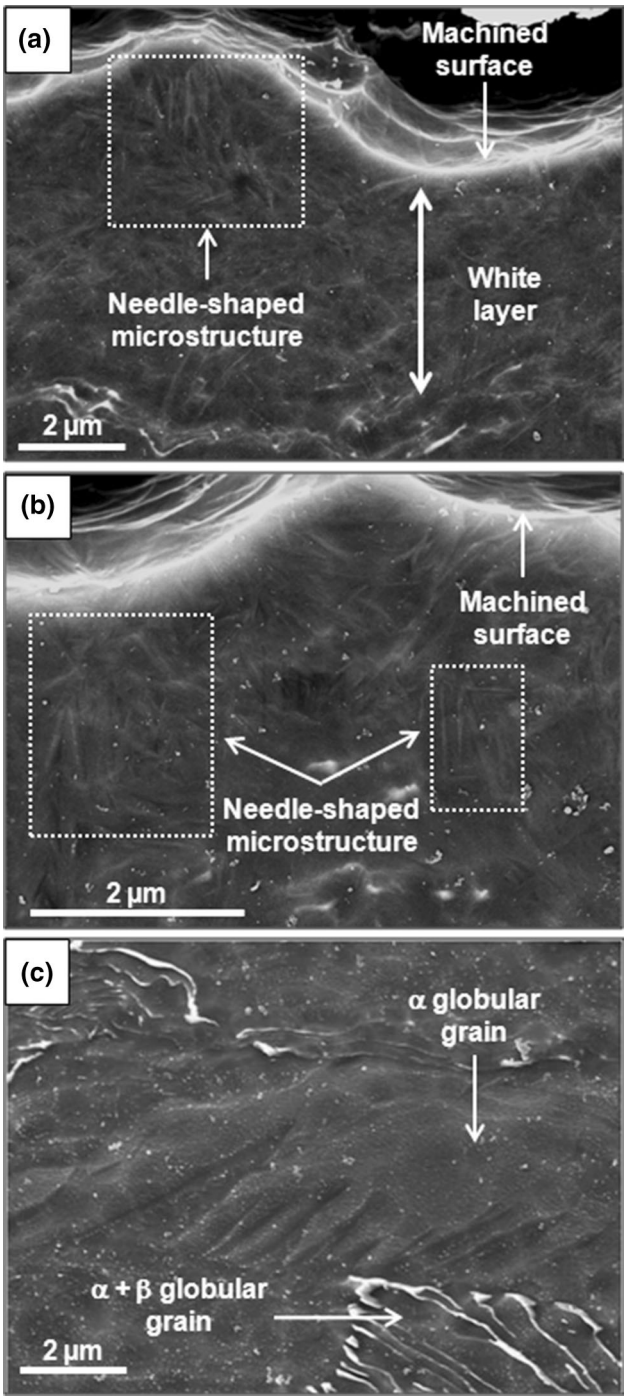

Fig. 2—SEM images of Ti-6Al-4V microstructure close to the machined surface (*a*, *b*) and within the undamaged zone (*c*).

single-phase layer is constant (6.40 Al- and 3.86 V-pct) and is different from that of the α and β phases. Moreover, it is close to the nominal composition of Ti-6Al-4V, defined in Table II. This implies that a local dissolution of the material occurred during machining, *i.e.*, that the cutting temperatures attained during machining in the white layer exceeded the β-transus [>1283 K (1010 °C)] before the material was quenched.

The chemical composition of the single-phase layer shows that it could be composed of βm, αm, or martensitic (α' or α'') phases. According to Le Maître,[18–20] whatever the cooling rate from the β domain, βm phases cannot be entirely retained at room temperature for Ti-6Al-4V, contrary to other titanium alloys which are rich in β elements. Moreover, Williams and Blackburn[21–23] pointed out that martensitic α'' is generated during rapid cooling from the $\alpha + \beta$ domain at a temperature of between 993 K and 1103 K (720 °C and 830 °C). Nevertheless, the increase in vanadium content in the β phase as a function of the increasing temperature prevents the generation of α'' after rapid quenching for $T > T_\beta$. As β_m and α'' cannot nucleate on the single-phase layer, α' and α_m are the only phases which could be generated.

C. *Transmission Electron Microscopy (TEM) Investigations*

1. *Bulk material*

Figure 4(a) presents a STEM-HAADF image (Z-contrast image) of a thin foil extracted from the bulk material. We can distinguish the two lamellar phases with respect to their mean atomic weight. The thinnest and brightest lamellas are the vanadium-rich β phases, while the thickest and darkest lamellas are the aluminum-rich β phases. The β lamellas have no defects, while dislocation networks are observed within the α lamellas, especially at the interface between the two phases, as illustrated in Figure 4(b). However, at this magnification, it is estimated that no sub-structures such as dislocation cells, twins, or recrystallized grains are detected.

EDX analysis in line-scan mode using a nanometric probe size was performed through both lamellar phases. The compositional profiles presented in Figure 4(c) reveal that the β phase contains a large amount of vanadium (~28 wt pct) and a low concentration of aluminum (3.8 wt pct). However, the chemical composition of the α phase is close to that determined by electron microprobe analysis. No investigation was conducted on α globular grains.

2. *Machined surface*

a. Single-phase layer. The microstructure within the single-phase layer is composed of recrystallized nanograins (Figure 5(b)), as observed by Li *et al.*[10,15] within the adiabatic shear band. The grain sizes range from 250 to 300 nm. These grains also contain twins, as illustrated by HRTEM imaging (Figure 5(c)). Needle-shaped phases, sometimes arranged as twins, are also detected (Figure 5(d)). This type of structure was also observed by Ahmed and Rack.[18,21] In both studies, this needle-shaped structure was induced by the rapid cooling of Ti-6Al-4V and corresponds to the martensitic phase.

The diffraction pattern obtained on the single-phase layer consists of rings in agreement with a polycrystalline structure. The indexation of the diffraction

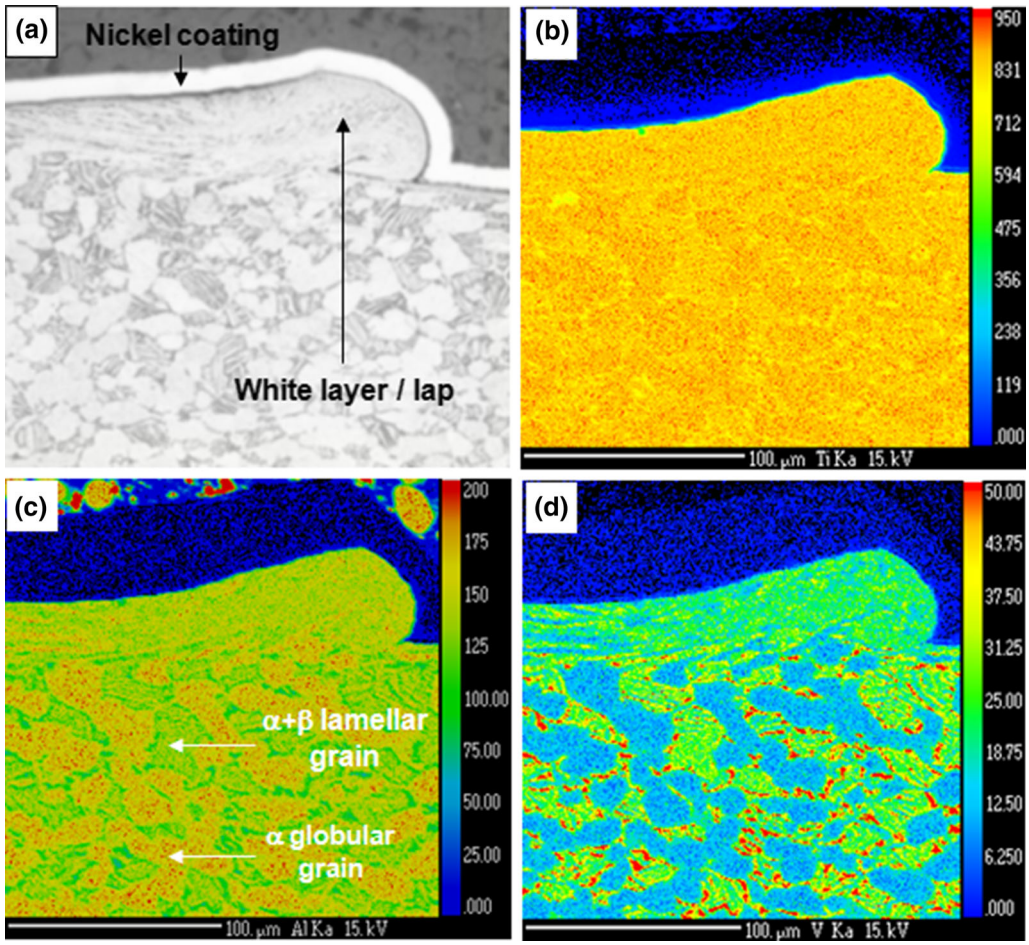

Fig. 3—(*a*) Optical image of the top layer showing a lap composed of the white layer. Electron probe cartographies of titanium (*b*), aluminum (*c*), and vanadium (*d*) within the white layer and the sublayer below the machined surface.

Table IV. Phases Chemical Composition Obtained by Electron Microprobe Analysis

	Phases			
Chemical Element (wt pct)	$\alpha_{globuar}$	$\beta_{lamellar}$	$\alpha_{lamellar}$	Single-Phased Layer
Ti	91.2 ± 0.24	83.4 ± 1.97	91.2 ± 0.28	89.7 ±0.59
Al	7.28 ± 0.04	3.85 ± 0.15	6.51 ± 0.16	6.40 ± 0.26
V	1.87 ± 0.07	12.2 ± 0.85	2.87 ± 0.13	3.86 ± 0.67
Fe	0.01 ± 0.02	0.86 ± 0.23	0.03 ± 0.02	0.14 ± 0.06

pattern reveals a hexagonal structure (P63/mmc) with $a = 0.295$ nm and $c = 0.468$ nm (Figure 5(e)). This result implies that recrystallized and disoriented grains were generated within this layer. From these results, and taking into account EPMA analyses, it is deduced that α' is the dominant phase in the single-phase layer.

b. Deformed layer. A TEM image of the deformed α-globular phase, localized below the single-phase layer, is presented in Figure 6(a). The microstructure is composed of recrystallized nanograins (≈100 nm) which are severely deformed with a high density of dislocations (Figure 6(b)). The diffraction pattern performed on a large area (~5 µm of diameter) shows almost continuous rings (inset in Figure 6(a)), which were indexed (not shown in the image) in agreement with the hexagonal structure (P63/mmc) of the α-Ti-6Al-4V phase. The continuous aspect of the diffraction rings (similar to the case of diffraction of nanometric powder) indicates the presence of a high density of very fine grains in this zone. This also indicates that the microstructure within the deformed layer is not textured (no preferential direction). These results are similar to those already obtained by Li *et al.*[10,14] on recrystallized grains localized within the adiabatic shear band in titanium alloys which have undergone a high strain rate loading test. They suggested that dynamic recrystallization occurred due to the significant deformation and heat induced during testing.

Figures 7(a) and (b) presents two TEM images acquired at different magnifications on the lamellar grain

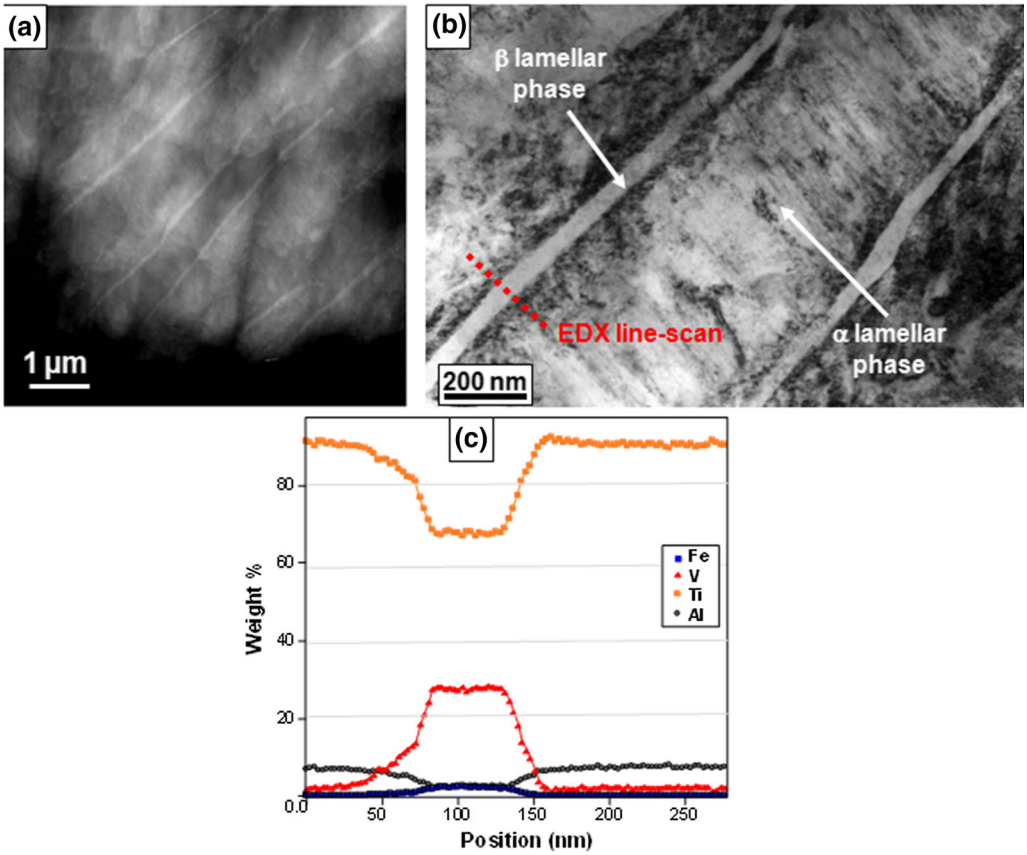

Fig. 4—HAADF (*a*) and TEM (*b*) micrographs of the thin foil extracted from the undamaged zone in the bulk material. (*c*) Compositional profiles calculated from EDX line-scan analysis performed through both lamellar phases (*b*) using a nanometric probe size.

region within the deformed layer. The diffraction pattern acquired in this zone (see inset in Figure 7(a)) indicates a fine-grained polycrystalline microstructure. Comparison with the $\alpha + \beta$ grains within the undamaged zone in the bulk material (Figure 4(b)) suggests that the thickest lamellas are α phase and the thinnest ones are β. However, as severe machining conditions could cause microstructure rearrangements and generate metallurgical transformations, the thickest and thinnest lamellas could not be α and β phase, respectively.

Many twins are formed in the thickest lamellas, which also contains a high density of dislocations. The twinning plane is {10-11}. This deformation accommodation was already detected in the α lamellar phase in Ti-6Al-4V by Karaman *et al.*[24] during Equal Channel Angular Extrusion (ECAE) testing. According to the authors, the rapid deformation rate ($\dot{\varepsilon} = 2\ s^{-1}$) and the significant shear deformation ($\tau = 120$ pct) of the material at high temperature [1073 K (800 °C)] induce this kind of twin. The thinnest lamellas have fewer defects than the thickest ones. Indeed, only a low dislocation density is visible. This is surprising, because if it is assumed that thinnest lamellas corresponds to the β phase, they should contain more defects due to their cubic structure compared to the hexagonal structure of the α lamellas. The response is given by HRTEM imaging combined with Fourier transform analysis (Figure 7(c)), which reveals that both phases are hexagonal. Thus, thinnest lamellas do not correspond to a β structure.

In order to determine the nature of thinnest lamellas, TEM-EDX analysis in line-scan mode was performed through both lamellar phases using a nanometric probe. The compositional profiles obtained are shown in Figure 8. Average concentration values calculated from compositional profiles are given in Table V.

These results are compared to those of lamellar phases in the bulk material. It is worth nothing that the chemical composition of thickest lamellas is close to that measured for the α phase in the bulk material. This result confirms that thickest lamellas are α phase which has undergone significant loading, inducing in particular a mechanical twinning.

Thinnest lamellas have the same chemical composition as the β lamellas located in the undamaged zone (comparison between Tables IV and V) but do not have the same crystallographic structure. This demonstrates that a metallurgical transformation without diffusion occurred in the original β phase during machining. Considering this result, thinnest lamellas are orthorhombic α'' or hexagonal α' phase. As the crystallographic structure of these lamellas is hexagonal, the thinnest ones are α' phase.

IV. DISCUSSION

A. *Single-Phase Layer*

The single-phase layer generated just below the machined surface was induced by temperature. This

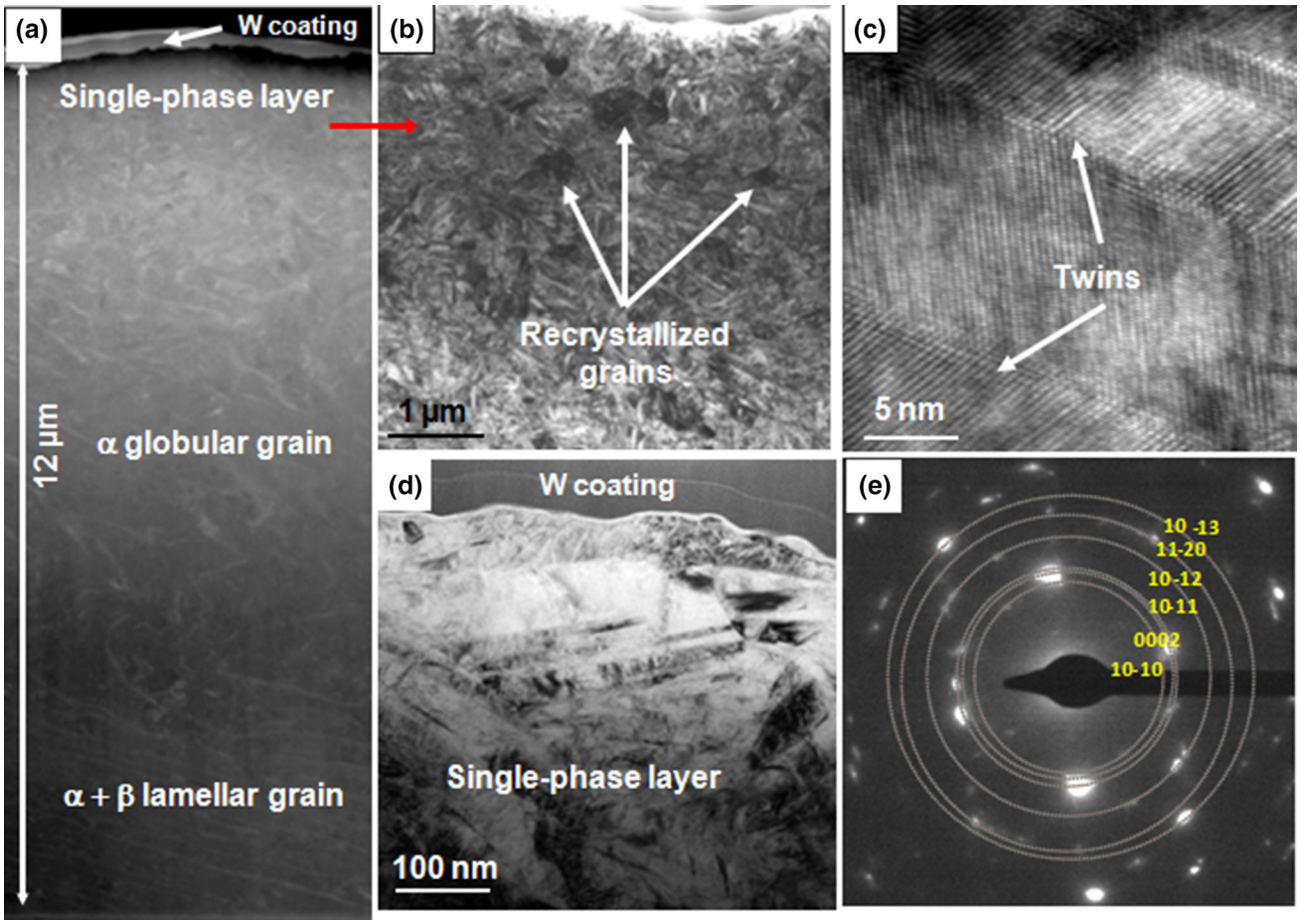

Fig. 5—(*a*) HAADF image of thin foil extracted by FIB from the machined surface; (*b*) TEM image obtained in a region within the single-phase layer; (*c*) HRTEM image of a recrystallized grain; (*d*) Needle-shaped grains detected in the single-phase layer; (*e*) Diffraction pattern of the single-phase layer revealing a hexagonal structure (P63/mmc) with $a = 0.295$ nm and $c = 0.468$ nm.

layer appeared after the increase in temperature above the β-transus leading to the whole dissolution of the material. This temperature increase was followed by a rapid quenching of the material and the formation of the α' during cooling. Moreover, the high mechanical loading due to machining created a large network of dislocations. The significant deformation rate (between 10^2 and 10^5 s^{-1}[25]) enabled the increase in temperature, inducing a restoration followed by a dynamic recrystallization of the material.

It has been shown in the studies of MeBar and Shechtman[8,10,14,26] that the adiabatic shear band consists of a white layer with a recrystallized microstructure revealed after chemical etching. As the single-phase layer has the same characteristics, it is concluded that this layer is an adiabatic shear band commonly observed in the primary and secondary shear zones of chips.[7] The present study shows that this damage can be induced in the third adiabatic shear zone of the machined Ti-6Al-4V material during turning.

The microstructures observed by different authors in the adiabatic shear band formed after high strain rate test on Ti-6Al-4V or titanium alloys are summarized in Table VI. This comparison indicates that recrystallized grains are observed in all of the studied microstructures. However, contrary to the findings of Xu *et al.*,[13,14] no twins were observed within the adiabatic shear band. Moreover, no metallurgical transformation was detected by any other authors, contrary to the results in the present study.

B. *Deformed Layer*

The mechanism leading to the formation of a recrystallized structure in the α-globular grains is approximately the same as in the white layer. The large amount of heat due to the rapid deformation of the material induced the restoration of dislocations and the dynamic recrystallization of nanograins. No metallurgical transformation was observed in these grains, even if they were partially dissolved.

In the case of the lamellar grains, no dissolution occurred because the chemical compositions of the lamellas were close to those of the bulk material. Moreover, a metallurgical transformation without diffusion from β to α' phases was observed. This transformation is attributed to thermal loading, since the material underwent a rapid increase in temperature and then rapid quenching. In these conditions, Ahmed and Rack[18,20,21,23] have proved that

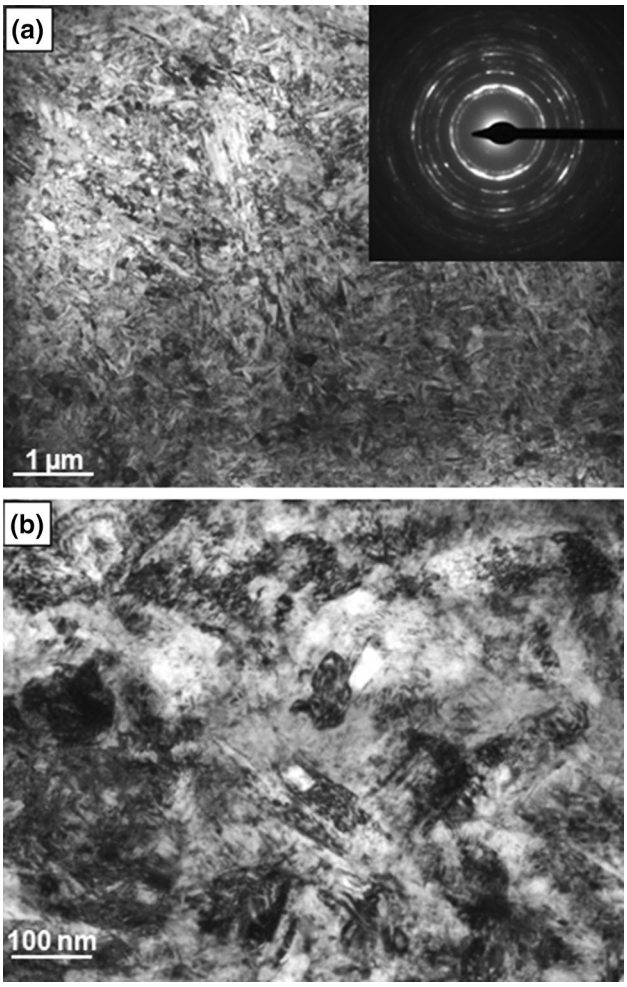

Fig. 6—(*a*) TEM image of a region within a α globular grain close to the machined surface. The insert is the corresponding diffraction pattern. The diffracted rings were indexed (not shown in the image) in agreement with the hexagonal structure (P63/mmc) of the α-Ti-6Al-4V phase. (*b*) Zoom of the central area in Figure (*a*) showing heavily deformed grains.

- for $T < T_\beta$, α and α′ phases cannot be generated without the presence of β_m within Ti-6Al-4V lamellar grains
- a large amount of α phase cannot be obtained after rapid quenching from a temperature above the β-transus.

It can be concluded that this metallurgical transformation is not due to thermal loading, but is mainly due to mechanical loading. We can note that this type of transformation depends on the crystallographic structure and on the chemical composition of the phase. In particular, an investigation of the undamaged zone revealed that the β-phase was rich in vanadium. If this phase were considered as a titanium alloy, it would be a β-metastable according to the classification of Combres,[27] depending on $[Mo]_{eq}$ and $[Al]_{eq}$ (Table VII). The Ms temperature of β-metastable alloy is below room temperature, preventing the formation of the α′ phase during rapid quenching. Nonetheless α′ can be formed in β-metastable titanium alloy during mechanical loading. This mechanism was also observed by Koul and Breeds[28] in titanium alloy containing elements which extend the β-domain: Ti-13 wt pct, Mo and Ti-16 wt pct V. The large deformation of the α-lamellas adjacent to α′ lamellas confirms that lamellar grains underwent significant mechanical loading during machining. Thus this mechanical loading induced the metallurgical transformation from the vanadium-rich β phase to the α′ phase.

The microstructures observed by different authors within the deformed layer after high strain rate tests on Ti-6Al-4V or titanium alloys are summarized in Table VIII. Recrystallized grains (especially in the α phase), twins, and grains with a high density of dislocations are observed in the deformed layer. This damage is the same as that observed in the deformed layer generated in the present study.

The same observations were reported by Landau *et al.*[15] concerning metallurgical transformation. α′ phase was detected at the location of the former β phase; this transformation being induced by mechanical loading. Moreover, the authors detected an α″ martensitic phase, contrary to the present study. MeBar and Shechtman[8,9,12] have observed hatched martensitic structures within Ti-6Al-4V, and Xu *et al.*[14] have detected α_2 phase in α phase. This kind of metallurgical transformation was not detected in the present study.

This difference between the metallurgical transformations obtained in the present study (α′ detected) and those observed elsewhere (α″ or α_2 detected) is not clearly understood. The chemical composition of Ti-6Al-4V phases and the microstructure (globular or lamellar phases) may explain these differences.

C. *Microstructural Evolution in the Sublayer During Machining*

Microstructural evolution mechanisms occurring in the deformed layer and in the single-phase layer are proposed below. The first step and the last step of each mechanism were previously observed, and assumptions are advanced in order to explain the microstructure evolution between these both steps.

1. *Deformed layer variations*

The mechanism of α-globular grain variations during machining is presented in Figure 9. Four steps describe the transformation of the microstructure. Steps 2α and 3α show the dynamic recrystallization inside the grains. This transformation is similar to those defined by Murr *et al.*[12] concerning the evolution of the microstructure within the adiabatic shear band in Ti-6Al-4V during high deformation rate testing.

The transformation mechanism of the α + β lamellar grains close to the machined surface is presented in Figure 10. Four steps also described the microstructure transformation. Plastic deformation induced during cutting generates a high density of dislocations in the α and β phases (step $2_{\alpha+\beta}$). Moreover, the combination of this deformation and mechanical loadings leads to the twinning of the α phase. The transition between steps

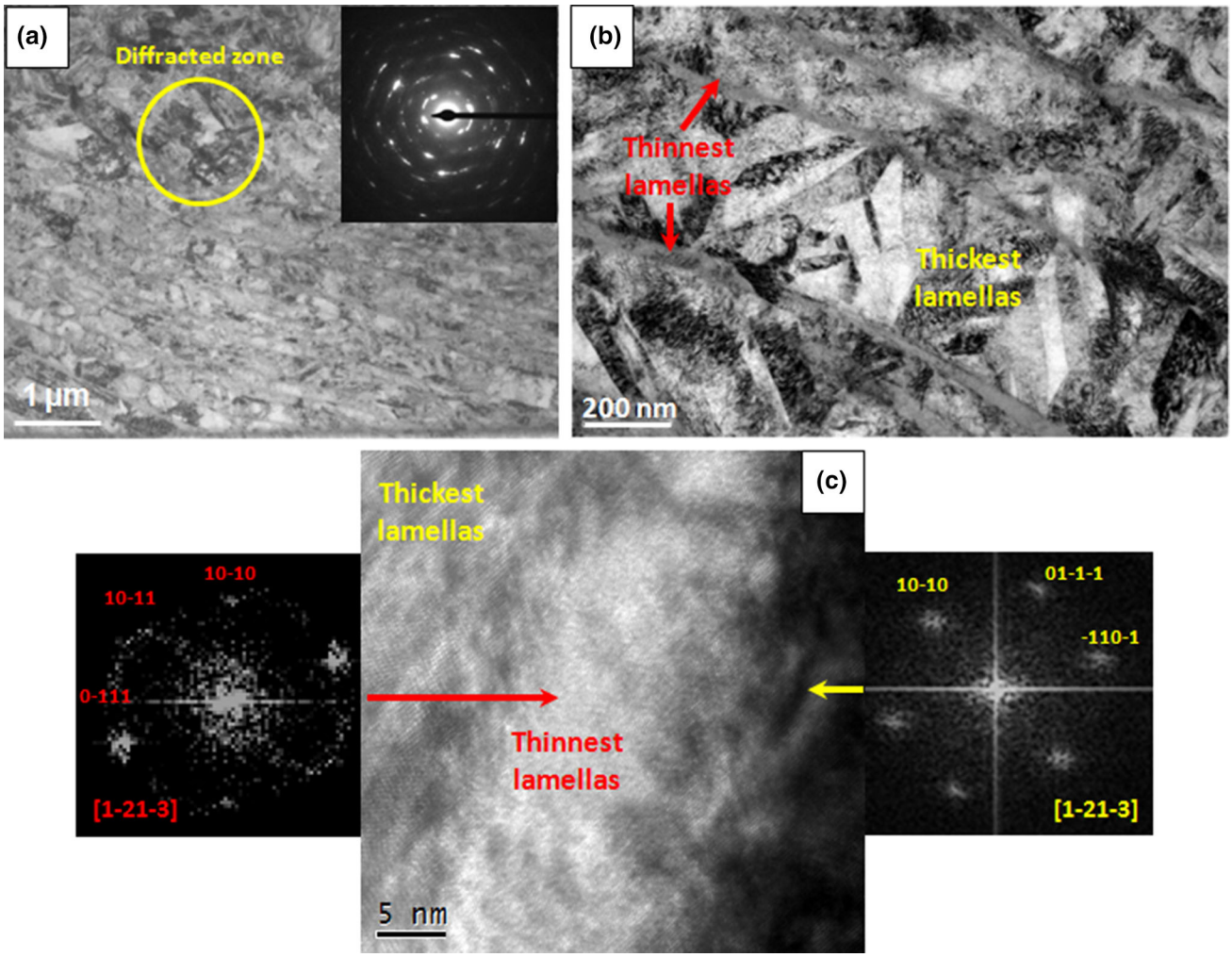

Fig. 7—(*a*) and (*b*) TEM images acquired at different magnifications of the lamellar grain region within the deformed layer. The insert in (*a*) is the diffraction pattern acquired on the surrounded zone. (*c*) High-resolution image of lamellar phases. Analysis of the local Fourier transforms highlights the hexagonal structure of both phases.

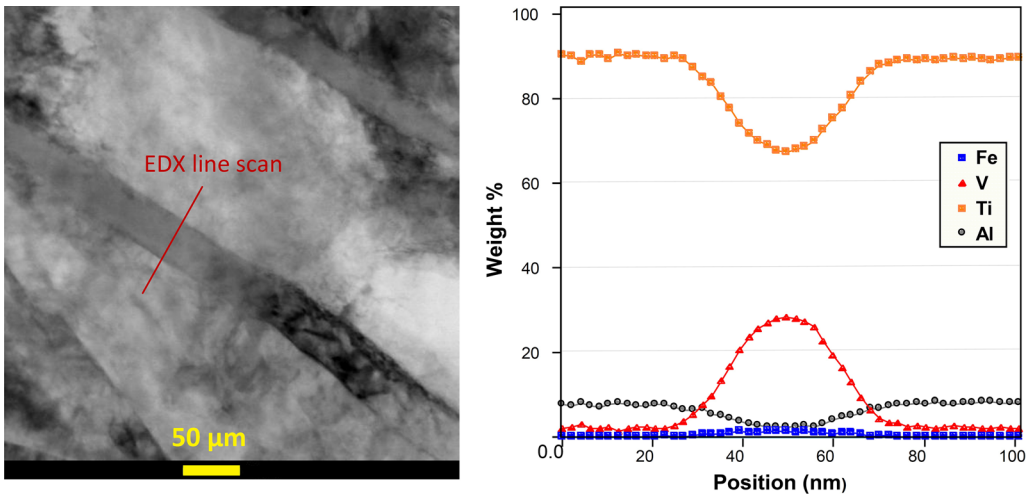

Fig. 8—(*a*) STEM bright-field image of lamellar phases. (*b*) Compositional profiles calculated from EDX line-scan analysis performed through both lamellar phases using a nanometric probe size.

Table V. Chemical Composition Comparison Between Lamellar Phases of a Grain Localized in Bulk Material and Lamellar Phases of a Grain Placed Close to Machined Surface

	Lamellar Grain in Bulk Material (Figure 4)		Lamellar Grain Close to Machined Surface (Figure 8)	
Chemical Element (wt pct)	$\alpha_{lamellaire}$	$\beta_{lamellaire}$	Phase 1	Phase 2
Ti	89.9 ± 0.68	67.8 ± 0.8	89.5 ± 0.64	68.1 ± 0.89
Al	7.1 ± 0.24	3.8 ± 0.11	7.7 ± 0.44	2.8 ± 0.22
V	2.9 ± 0.64	27.7 ± 1.31	2.6 ± 0.63	27.5 ± 0.91
Fe	0.07 ± 0.11	1.7 ± 0.33	0.17 ± 0.13	1.5 ± 0.24

Table VI. Summary of Metallurgical and Microstructural Evolutions Observed in the Single-Phased Layer-Comparison with the Results of Other Studies

Authors	Metallurgical Transformation	Microstructural Evolution	$\dot{\varepsilon}$ (s^{-1})	ε
Li *et al.*[10]		low density of dislocations and generation of small equiaxial grains	10^6	
Xu *et al.*[13]		twinning (size of twins: nanometric)	10^3	
Xu *et al.*[14]		high density of dislocations and generation of twins, micro-twins and dislocations cells	10^4	
Landau *et al.*[15]		high density of dislocations and generation of recrystallized nanograins and large amount of cells	3.10^5	45 pct
The present study	generation of martensitic α' phase from bimodal microstructure	generation of recrystallized nanograins (≈250 nm) including a high density of dislocations and martensitic α' phase. Sometimes this phase is twinned. The nanometric grains are disorientated	?	?

Table VII. Classification of Titanium Alloys and Identification of β Lamellar Class

		$\beta_{lamellar}$	
Titanium Alloys Classification	Criteria	$[Mo]_{eq}$ (pct)	a + b $[Al]_{eq}$ (pct)
α et quasi α alloys	$[Mo]_{eq} < 1 + 0.125\ [Al]_{eq}$	23.1	1.5
$\alpha + \beta$ alloys	$[Mo]_{eq} > 1 + 0.125\ [Al]_{eq}$	23.1	1.5
β rich alloys	$[Mo]_{eq} > 6 + 0.5\ [Al]_{eq}$	23.1	7.9
β métastable alloys	$[Mo]_{eq} > 10 + [Al]_{eq}$	23.1	13.8
β stable alloys	$[Mo]_{eq} > 27 + [Al]_{eq}$	23.1	30.8

$2_{\alpha+\beta}$ and $4\alpha_{+\beta}$ observed by TEM is not straight, according to several authors. In particular, the studies of Landau *et al.*[15,29] concerning the metallurgical transformation, respectively, in Ti-6Al-4V and β-metastable titanium alloy show that the martensitic α' and α'' phases can be generated by mechanical loading. Moreover, Nwobu *et al.*[30,31] have determined that α'' and α' appear within the β phase as a function of the increase in plastic deformation in β-metastable titanium, following the scheme: $\beta \rightarrow \alpha'' \rightarrow \alpha'$. Transition step III should consist of the formation of α'' in the β phase prior to the formation of α'.

The $\beta \rightarrow \alpha''$ transformation was not observed by TEM. It is supposed that the sublayer close to the machined surface has undergone too large a plastic deformation, inducing the following transformation: $\beta \rightarrow \alpha'' \rightarrow \alpha'$. In order to demonstrate that the $\beta \rightarrow \alpha''$ transformation occurred, a thin foil should be taken from the deep deformed sublayer, as performed by Landau *et al.*[15] In fact, the authors detected the α'' phase at a distance of between 20 and 50 μm from the adiabatic shear band. In the present paper, the thin foil extracted by FIB from the machined surface enabled us to study only the first ten micrometers below the

Table VIII. Summary of Metallurgical and Microstructural Evolution Observed in Deformed Layer-Comparison with Other Studies

Authors	Metallurgical Transformation	Microstructural Evolution	$\dot{\varepsilon}$ (s^{-1})	ε
MeBar and Shechtman[8]	generation of grains which have a hatched appearance. This hatched structure is α' needle	α recrystallized structure β ellongated phase α rows of dislocations and twins parallel to the following plane (1-211) and (0-111) β rows of dislocations	3.10^5	
Grebe *et al.*[9]				
Murr *et al.*[12]			10^5	
Li *et al.*[10]		high density of dislocations and generation of twins	10^6	
Xu *et al.*[13]		generation of twins	10^3	
Xu *et al.*[14]	*from* α *phase* generation of α_2 phase		10^4	
Landau *et al.*[15]	*from* β *phase* generation of α' et α'' phases due to mechanical loading	generation of cells and recrystallized grains included density of dislocations	3.10^5	45 pct
The present study	*from* $\alpha_{lamellar}$ generation of α' phases due to mechanical loading	*from* $\alpha_{lamellar}$ generation of twins included a high density of dislocations. The reticular plan of the twin is (10 to 11) *from* $\alpha_{globular}$ recrystallized and disorientated grains included a high density of dislocations. The size of the grains is approximatively 100 nm	?	?

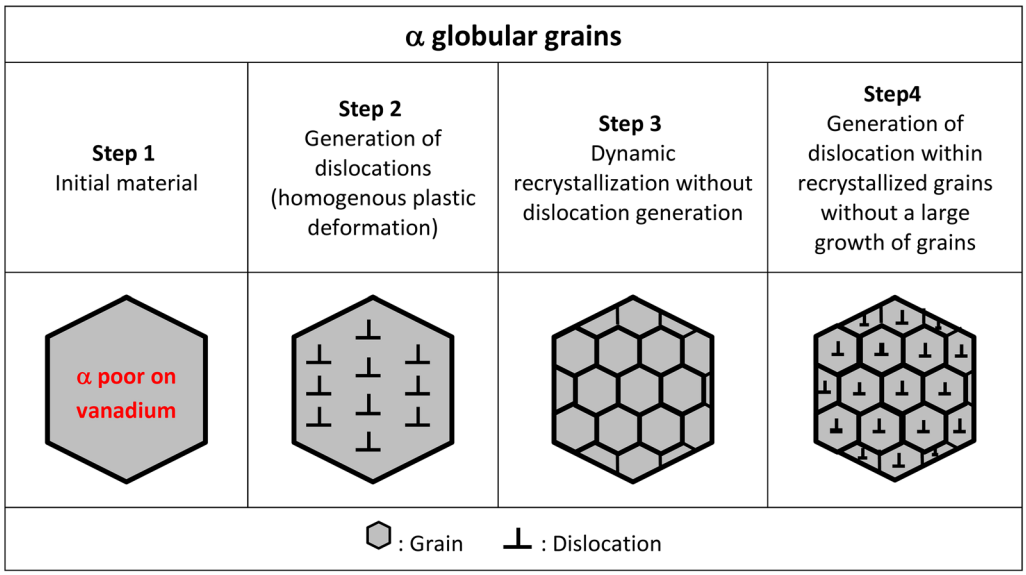

Fig. 9—Transformation of α globular grains close to the machined surface.

adiabatic shear band (single-phase layer). Additionally, step $3\alpha_{+\beta}$ remains to be confirmed in a forthcoming investigation.

2. *Single-phase layer variations*

The investigations performed by Li *et al.*[10,13] show that the adiabatic shear band is generated from the deformed layer in titanium alloys during high deformation rate testing. As the microstructure of globular and lamellar grains presented in steps 4α and $4\alpha_{+\beta}$ corresponds to the final metallurgical state of the deformed layer, it could be considered as a transition step leading to the formation of the single-phase layer. Based on this assumption, Figure 11 presents the different steps of the Ti-6Al-4V transition from the deformed to the single-phase layer.

Step $1_{\alpha-\alpha+\beta}$ is representative of the most deformed layer observed by TEM. This microstructure is composed of steps 4_{α} and $4_{\alpha+\beta}$. As the chemical composition of the single-phase layer is homogeneous and is similar to the nominal Ti-6Al-4V composition, dissolution of the α' (rich in vanadium) and α (rich in aluminum) phases has occurred. This implies that the temperature at the single-phase layer location exceeds the β-transus.

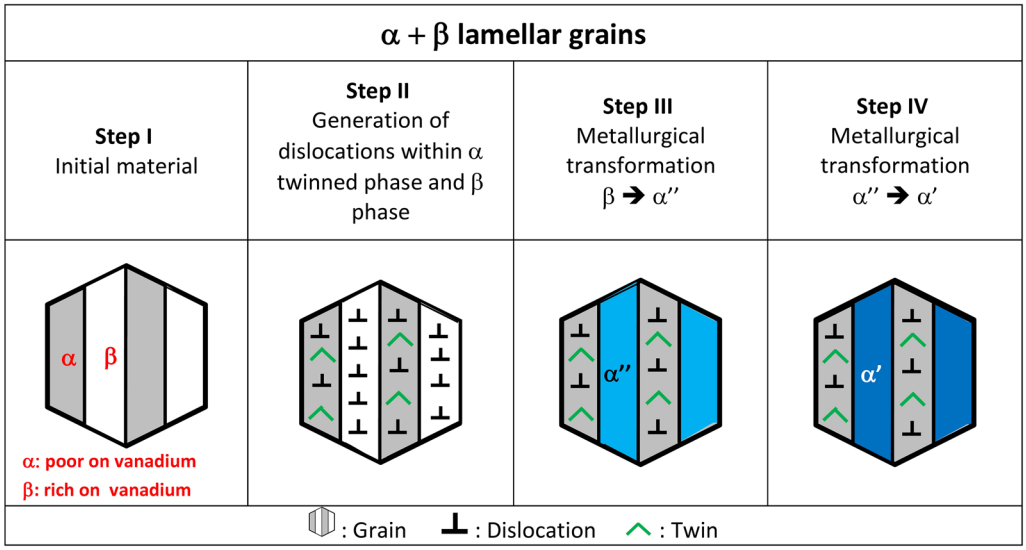

Fig. 10—Transformation of $\alpha + \beta$ lamellar grains close to the machined surface.

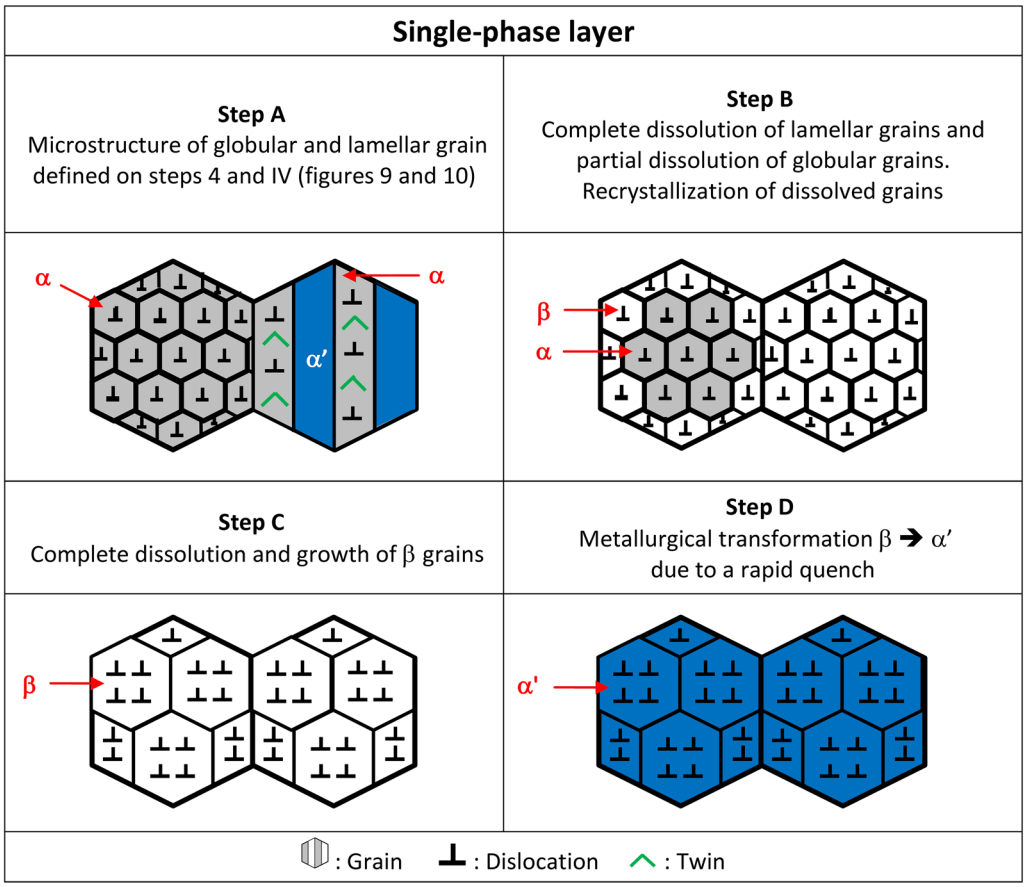

Fig. 11—Transformation of Ti-6Al-4V from deformed layer to single-phased layer.

The manner in which dissolution occurs was not observed.

Nevertheless, within the deformed layer, in the vicinity of the single-phase layer, the lamellar grains have undergone significant dissolution, contrary to the globular grains, and are sometimes no longer visible. This result shows that the dissolution of lamellar grains occurred before that of globular grains. This mechanism, leading to the metallurgical transformations $\alpha \rightarrow \beta$ and $\alpha' \rightarrow \beta$, is represented in step $2_{\alpha-\alpha+\beta}$. The localized high deformation coupled with the high temperature in the single-phase layer (equivalent to the

adiabatic shear band in this study) implies a dynamic recrystallization of the grains. As this recrystallization generally occurs between 0.4 and 0.5 T_f [773 K and 958 K (500 °C and 685 °C) for Ti-6Al-4V], it could be assumed that the dissolution of the different phases begins during the transition from step $1_{\alpha-\alpha+\beta}$ to step $2_{\alpha-\alpha+\beta}$.

Step $3_{\alpha-\alpha+\beta}$ shows the complete dissolution of the globular grains. At this step, the temperature within the single-phase layer is above the β-transus [more than 1273 K (1000 °C)]. According to Gil *et al.*,[32] at this temperature, the growth of β grains is faster than that of α grains. This result is in agreement with the TEM observations: the recrystallized grains visible in the single-phase layer (250 nm) are larger than the globular grains (100 nm) in the deformed layer.

Step $4_{\alpha-\alpha+\beta}$ defines the last metallurgical transformation of the material within the sublayer close to the machined surface: the quenching of the Ti-6Al-4V from the β domain. MeBar and Shechtman[8] have calculated that the cooling rate in the adiabatic shear band is approximately 10^7 K/s (10^7 °C/s). Moreover, Ahmed and Rack[18] showed that a cooling rate above 798 K/s (525 °C/s) from the β domain generates a martensitic α' acicular microstructure. This rapid quenching from the β domain (transition between steps $3_{\alpha-\alpha+\beta}$ and $4_{\alpha-\alpha+\beta}$) generates the α' microstructure within the sublayer close to machined surface and maintains the size of grains unchanged, as at high temperatures. The origin of the large number of dislocations could come from the martensitic transformation or from the mechanical loading induced by machining. Nevertheless, no metallurgical proof was observed by TEM to enable us to determine the way these dislocations were formed.

V. CONCLUSIONS

In this study, anomalies generated close to the turned surface of Ti-6Al-4V were investigated by SEM, EPMA, and especially by TEM. The main results of the present paper are the following:

1. Homogeneous metallurgical transformations are observed within the sublayer at the vicinity of the machined surface. The white layer generated during machining is due to the thermomechanical loading undergone by the material. This white layer is a single-phase layer mainly composed of α' and of dynamic recrystallized disoriented nanograins ($\approx$250 nm). These characteristics imply that the single-phase layer is an adiabatic shear band similar to those generated in the primary and secondary adiabatic shear bands on the chip.
2. Metallurgical and microstructural transformations are observed in the deformed layer below the single-phase layer. Recrystallized nanograins ($\approx$100 nm) and large number of dislocations are visible within the whole α globular grains. No metallurgical transformation is observed in these grains, contrary to $\alpha + \beta$ grains, where a second-order transformation $\beta \rightarrow \alpha'$ occurred due to local mechanical loadings. The α lamellas undergo significant thermomechanical loading, leading to twinning and the formation of a high concentration of dislocations in this phase.
3. Different steps in the microstructural and metallurgical evolution of the deformed layer are proposed according to the study results and assuming several hypotheses. The transformation of the globular grains consists of classic dynamic recrystallization, as described by Murr *et al.*,[12] in the Ti-6Al-4V adiabatic shear band. The main evolution consists of the metallurgical transformation of the lamellar β phase. It is supposed that first the appearance of the α'' martensitic phase from the β phase is due to local mechanical loading. An increase in this loading then leads to the transformation $\beta \rightarrow \alpha'$.
4. A driving mechanism for the generation of the single-phase layer from the deformed layer is proposed according to the study results and assuming several hypotheses. It consists of the complete dissolution of the α' or α phases and the formation of the β phase followed by the growth of the grains due to dynamic recrystallization (similar to the globular α phase in the deformed layer). This mechanism is supposed to be activated by significant mechanical loading close to the turned surface and a rapid increase in temperature above the β-transus. The rapid decrease in temperature leads to α' phase generation.

ACKNOWLEDGMENTS

The authors would like to acknowledge the financial support provided by the European Union for the FP7-AAT- 2007- RTD-1 ACCENT project. Additional thanks go to Snecma Evry-Corbeil for their technical advice and funding for the study.

REFERENCES

1. E.O. Ezugwu and Z.M. Wang: *J Mater. Process. Technol.*, 1997, vol. 68, pp. 262–74.
2. E.O. Ezugwu, J. Bonney, and Y. Yamane: *J Mater. Process. Technol.*, 2004, vol. 134, pp. 233–53.
3. T. Kitagawa, A. Kubo, and K. Maekawa: *Wear*, 1997, vol. 202, pp. 142–48.
4. C.H. Che-Haron and A. Jawaid: *J Mater. Process. Technol.*, 2005, vol. 166, pp. 188–92.
5. J.L. Cantero, M.M. Tardio, J.L. Canteli, M. Marcos, and M.H. Miguélez: *Int. J. Mach. Tools Manuf.*, 2005, vol. 45, pp. 1246–55.
6. J.D.P Velasquez: Etude des copeaux et de l'intégrité de surface en usinage à grande vitesse de l'alliage de titane TA6V, Thèse Ecole Nationale d'Ingénieurs de Metz, 2007.
7. Z.P. Wan, Y.E. Zhu, H.W. Liu, and Y. Tang: *Mater. Sci. Eng. A*, 2012, vol. 531, pp. 155–63.
8. Y. MeBar and D. Shechtman: *Materi. Sci. Eng.*, 1983, vol. 58, pp. 181–88.
9. H.A. Grebe, H.R. Pak, and M.A. Meyers: *Metall. Trans. A*, 1985, vol. 16A, pp. 761–75.
10. G.A Li, L. Zhen, C. Lin, R.S. Gao, X. Tan, and C.Y. Xu: *Materi. Sci. Eng. A*, 2005, vol. 395, pp. 98–101.

11. F. Martinez, L.E. Murr, A. Ramirez, M.I. Lopez, and S.M. Gaytan: *Materi. Sci. Eng. A*, 2007, vol. 454, pp. 591–99.
12. L.E. Murr, A.C. Ramirez, S.M. Gaytan, M.I. Lopez, E.Y. Martinez, D.H. Hernandez, and E. Martinez: *Materi. Sci. Eng. A*, 2009, vol. 516, pp. 205–16.
13. Y.B. Xu, L. Liu, J.Q. Yu, L.T. Shen, and Y.L. Bai: *Mater. Sci. Technol.*, 2000, vol. 16, pp. 609–11.
14. Y. Xu, Y. Bai, and M.A. Meyers: *J. Mater. Sci. Technol.*, 2006, vol. 22, pp. 737–46.
15. P. Landau, A. Venkert, and D. Rittel: *Metall. Mater. Trans. A*, 2010, vol. 41, pp. 389–96.
16. S. Lampman: Titanium and Titanium Alloys. in Properties and Selection: Nonferrous Alloys and Special-Purpose Materials, ASM Handbook, vol 2, 1990, pp. 593–633.
17. Y.K. Chou and C.J. Evans: *Trans. SME*, 1998, vol. 26, pp. 117–22.
18. T. Ahmed and H.J. Rack: *Mater. Sci. Eng. A*, 1998, vol. 243, pp. 206–11.
19. F.L. Maitre: Etude des transformations en refroidissement continu de l'alliage de titane TA6V*Mémoires Scientifiques de la Revue de Métallurgie*, 1970, vol. 67, pp. 563–74.
20. M.T. Jovanovic, S. Tadic, S. Zec, Z. Miskovic, and L. Bobic: *Mater. Des.*, 2006, vol. 27, pp. 192–99.
21. J.C. Williams and M.J. Blackburn: *Trans. ASM*, 1967, vol. 60, pp. 373–83.
22. B. Hocheid, R. Klima, C. Beauvais, M. Rapin, and C. Roux: *Mémoires Scientifiques de la Revue de Métallurgie*, 1970, vol. 68, pp. 583–90.
23. Y.T. Lee and G. Welsch: *Mater. Sci. Eng. A*, 1990, vol. 128, pp. 77–89.
24. I. Karaman, G.G. Yapici, Y.I. Chumlyakov, and I.V. Kireeva: *Mater. Sci. Eng. A*, 2005, vols. 410–411, pp. 243–47.
25. T. Braham: Etude du comportement en sollicitations extrêmes et de l'usinabilité d'un nouvel alliage de titane aéronautique : le Ti555-3, Thèse Ecole Nationale Supérieure d'Arts et Métiers d'Angers, 2010.
26. S.P. Timothy and I.M. Hutchings: *Acta Metall.*, 1985, vol. 33, pp. 667–76.
27. Y. Combres and B. Champin: Traitements thermiques des alliages de titane, Techniques de l'Ingénieur, 1995, M1335.
28. M.K. Koul and J.F. Breedis: *Acta Metall.*, 1970, vol. 18, pp. 579–88.
29. S. Ishiyama, S. Hanada, and O. Izumi: *Sumitomo Search*, 1993, vol. 54, pp. 41–47.
30. A.I.P. Nwobu, H.M. Flower, and D.R.F West: *J. Phys.*, 1982, vol. 43, pp. 315–20.
31. T. Grosdidier, C. Roubaud, M.J. Philippe, and Y. Combres: *Scr. Mater.*, 1997, vol. 36, pp. 21–28.
32. F.J. Gil, M.P. Ginebra, J.M. Manero, and J.A. Planell: *J. Alloys Compd.*, 2001, vol. 329, pp. 142–52.